Regenerative Therapy 16 (2021) 12–22

Contents lists available at ScienceDirect

Regenerative Therapy

journal homepage: http://www.elsevier.com/locate/reth

Original Article

Bone formation potential of collagen type I-based recombinant peptide particles in rat calvaria defects☆

Yasunori Akiyama [a], Masaaki Ito [a], Taku Toriumi [b], Takahiro Hiratsuka [c], Yoshinori Arai [d], Sho Tanaka [b], Taku Futenma [b], Yuhki Akiyama [a], Kazuhiro Yamaguchi [c], Akihiko Azuma [c], Ken-ichiro Hata [c], Nagato Natsume [a], Masaki Honda [b, *]

[a] Division of Research and Treatment for Oral and Maxillofacial Congenital Anomalies, School of Dentistry, Aichi Gakuin University, 2-11 Suemori-dori, Chikusa-ku, Nagoya, Aichi, 464-8651, Japan
[b] Department of Oral Anatomy, School of Dentistry, Aichi Gakuin University, 1-100 Kusumoto-cho, Chikusa-ku, Nagoya, Aichi, 464-8650, Japan
[c] Bio Science & Engineering Laboratory, Research & Development Management Headquarters FUJIFILM Corporation, 577 Ushijima, Kaisei-machi, Ashigarakami-gun, Kanagawa, 258-8577, Japan
[d] Department of Oral and Maxillofacial Radiology, Nihon University School of Dentistry, 1-8-13 Kanda-Surugadai, Chiyoda-ku, Tokyo, 101-8310, Japan

ARTICLE INFO

Article history:
Received 10 October 2020
Received in revised form
25 November 2020
Accepted 3 December 2020

Keywords:
Autologous bone
Bone reconstruction
Bone substitute
Calvaria
Collagen scaffold
Recombinant human collagen peptide

ABSTRACT

Introduction: This study aimed to examine the bone-forming ability of medium-cross-linked recombinant collagen peptide (mRCP) particles developedbased on human collagen type I, contains an arginyl-glycyl-aspartic acid-rich motif, fabricated as bone filling material, compared to that of the autologous bone graft.
Methods: Calvarial bone defects were created in immunodeficient rats though a surgical procedure. The rats were divided into 2 groups: mRCP graft and tibia bone graft (bone graft). The bone formation potential of mRCP was evaluated by micro-computed tomography and hematoxylin-eosin staining at 1, 2, 3, and 4 weeks after surgery, and the data were analyzed and compared to those of the bone graft.
Results: The axial volume-rendered images demonstrated considerable bony bridging with the mRCP graft, but there was no significant difference in the bone volume and bone mineral density between the mRCP graft and bone graft at 4 weeks. The peripheral new bone density was significantly higher than the central new bone density and the bottom side score was significantly higher than the top side score at early stage in the regenerated bone within the bone defects.
Conclusion: These results indicate that mRCP has a high potential of recruiting osteogenic cells, comparable to that of autologous bone chips.

1. Introduction

An alveolar cleft is a bone developmental defect in the alveolar process of the maxilla [1]. Its repair allows restoring maxillary bone continuity, inducing tooth eruption, improving orthodontic treatment outcome, and reconstituting the nasal cavity floor [2–4]. Alveolar cleft repair is frequently performed using cancellous autologous bone harvested from the iliac crest [2,4,5]. This procedure has several drawbacks associated with harvesting (e.g., chronic pain, infection, scar formation, hematoma, and nerve injury). Recently, various types of bone substitutes are being used for alveolar cleft repair [6–9]. However, use of bone substitutes has not shown superiority compared with autologous bone grafts [10,11]. Therefore, searching for novel bone substitutes is still

Abbreviations: RCP, recombinant collagen peptide; mRCP, medium-cross-linked RCP; RGD, arginyl-glycyl-aspartic acid; BMSCs, bone marrow derived mesenchymal stem cells; micro-CT, micro-computed tomography; BMD, bone mineral density; ROIs, regions of interest; H&E, hematoxylin and eosin; ALP, alkaline phosphatase; TRAP, tartrate-resistant acid phosphatase; SD, standard deviation; DHT, dehydothermal treatment; CSD, critical-size defect.

☆ This work was performed in Department of Oral Anatomy, School of Dentistry, Aichi Gakuin University, 1–100 Kusumoto-cho, Chikusa-ku, Nagoya, Aichi 464–8650, Japan.

* Corresponding author. Department of Oral Anatomy, School of Dentistry, Aichi Gakuin University, 1-100 Kusumoto-cho, Chikusa-ku, Nagoya, Aichi, 464-8650, Japan. Fax.: +81-52-752-5988
E-mail address: honda-m@dpc.agu.ac.jp (M. Honda).

Peer review under responsibility of the Japanese Society for Regenerative Medicine.

https://doi.org/10.1016/j.reth.2020.12.001

necessary for improving the clinical outcome in the surgical repair of alveolar cleft.

A three-dimensional bone substitute used for bone regeneration must be biodegradable, porous, and cytophilic. A porous bone substitute can retain cells within the defect site as well as function as a substrate for tissue ingrowth and vascularization. An ideal porous bone substitute should be biocompatible, non-inflammatory, non-immunogenic, and bioresorbable to be replaced with a matched biodegradation rate [12–16].

Because collagen type I is a major component of bone, collagen type I-based bone substitutes possess the requisite hemostatic properties, low antigenicity, and appropriate mechanical characteristics, and can promote cell and tissue attachment and growth [17]. However, conventional collagen scaffolds are obtained from xenogeneic tissues such as bovine and porcine tissues, which may increase the risk of unknown pathogens [18–24]. Hence, new collagen-based bone substitutes are needed to overcome the disadvantages of the collagen substrate source.

Recently, gene recombination technology has been introduced to counter the problem of xenogeneic materials [25,26]. A recombinant collagen peptide (RCP) designed using human collagen type I (α I chain), is commercially available from Fujifilm as Cellnest®; this RCP produced by a fermentation process using genetically modified yeast [27,28]. The collagen type I antigenic site has been removed from the RCP to reduce immunogenicity after implantation. Therefore, it poses no risk of infection from diseases such as bovine spongiform encephalopathy [22–24]. Further, as it can be manufactured massively, it is considered as a reproducible and consistent approach for bone regeneration.

In addition to no risk of infection, the RCP has several features as a bone substitute. First, the RCP is biodegradable and bioabsorbable; thus, it does not remain in the body. Second, the RCP contains 12 arginyl-glycyl-aspartic acid (RGD) motifs in a single molecule [29]. The RGD peptide is identified in extracellular matrix proteins such as vitronectin, fibronectin, and thrombospondin, as the minimal sequence required for recognition by cell membrane integrins [30–32]. The RGD motif is also found on chondrocytes, bone marrow-derived mesenchymal stem cells (BMSCs), and synovial MSCs [33–35]. RGD contributes to cell adhesion and osteoblastic differentiation [27–29,36]. Therefore, the RGD motif has been widely used to modify the surface of biomaterials for improved cell adhesion through augmented integrin interaction [37–39]. Re'em et al. further reported that the RGD peptide immobilized in alginate scaffolds facilitated chondrogenesis of BMSCs by promoting cell adhesion and proliferation [40,41]. These findings suggest that the RCP containing multiple RGD is expected to enhance cellular activities through integrin receptors.

Third, RCP materials have good biocompatibility as cellular scaffolds. Pawelec et al. showed that human MSCs could proliferate and differentiate on RCP materials [29]. A BMSC-RCP combination sponge construct was found to promote functional recovery post-implantation onto the ipsilateral intact neocortex for ischemic stroke [42]. When constructs of RCP sponge and MSCs were subcutaneously implanted into mice, MSCs were found to accelerate angiogenesis in the graft [27]. Mashiko et al. also showed that the RCP sponges could enhance the function of human adipose-derived stem cells in wound healing [43]. Our previous studies have demonstrated that RCP blocks can stimulate osteogenesis. New appositional bone formation is observed within RCP blocks upon grafting into an artificial created large bone defect at the inferior border of the rat mandible [44]. These results suggested that RCP materials can innovate bone regeneration therapy for alveolar cleft repair; however, the RCP block shape is not compatible with the large bone defect size of human alveolar cleft.

Finally, RCP has an extremely uniform molecular weight distribution of approximately 51 kD and is flexible; thus, it can be formulated into various forms, such as gels, sponges, granules, and porous particles. Formulation of porous particles was thus selected to examine the bone formation potential of RCP in this study because it is easy to implant the particles to the depth of the alveolar cleft in clinical settings.

Collagen-based materials also require an appropriate cross-linking density for controlling their property because cross-linking affects cellular activities [45–50]. To determine the optimal cross-linked RCP, three types of RCP particles with similar pore sizes were examined in our previous study. Micro-computed tomography (CT) and histological analyses indicated that the medium cross-linked RCP (mRCP) particles created a better environment prone to generate bone tissue compared to low or high cross-linked RCP particles (in submission). The present study aimed to determine whether the mRCP has a superior potential to regenerate bone compared to the autologous bone graft as a gold standard in a calvarial bone defect of critical size, based on micro-CT and histological analyses.

2. Materials and methods

2.1. Animals and housing

All experiments were performed using 9-week-old healthy male T cell-deficient rats with a bodyweight of 200–250 g (Chubu Kagaku Shizai, Nagoya, Japan). All the rats were kept at an animal experimentation laboratory at the Animal Research Center of Aichi Gakuin University, under standardized temperature and humidity with a 12-h day/night cycle. The study protocol was approved by the Animal Research Committee of the School of Dentistry, Aichi Gakuin University (approval No. AGUD412). Animal care and the experimental procedures were conducted in accordance with the

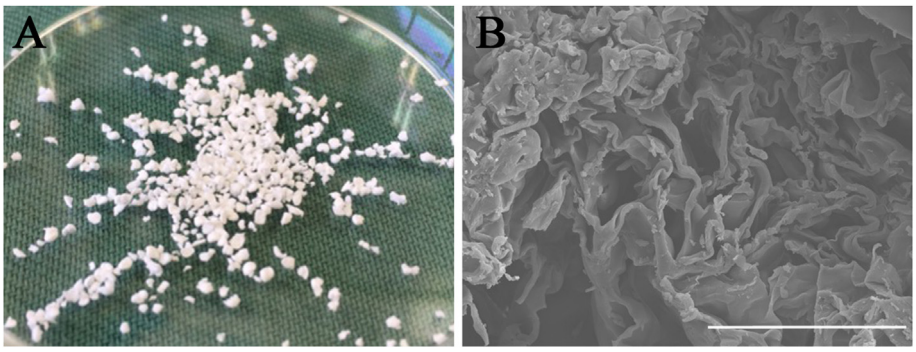

Fig. 1. (A) Gross appearance of medium-cross-linked recombinant collagen peptide (mRCP) particles with granular shape (B) A field-emission electron probe microanalyzer image of an mRCP particle. Scale bar represents 50 μm.

Regulations on Animal Experimentation at the School of Dentistry, Aichi Gakuin University.

2.2. Preparation of medium cross-linked recombinant collagen peptide (mRCP)

The RCP from human type I collagen α chain was prepared as described previously (FUJIFILM, Tokyo, Japan) [27–29,36,42–44]. After freeze-drying the RCP solution, porous RCP sponge blocks were cross-linked using a heat-dependent dehydration condensation reaction for 4.75 h, and were then crushed into particles to produce the mRCP (Fig. 1). The average diameter of the mRCP particle was approximately 1000 μm ranged from 1058 to 1133 μm.

2.3. Preparation of autologous bone chips

Autologous bones chips were taken from the tibia of T cell-deficient rats (9-week old). A 10-mm skin incision was made along the inferior border of the tibia, and the muscle and periosteum flap were elevated (Fig. 2A). Cortical and cancellous bone were collected from the tibia and then mixed (Fig. 2B); the mixed bone chips were cut into small pieces (0.5–1 mm) using an osteotome (Fig. 2C). These small pieces of tibial bone were immediately implanted into the bone defect in the same rats as in the autologous bone graft method.

2.4. Surgical procedure

The rats were anesthetized with 3.0% isoflurane (Mylan, Canonsburg, Pennsylvania, USA) in 30% oxygen and 70% nitrous oxide using a face mask and were allowed to breathe spontaneously. The head area was disinfected, a square skin incision was performed on the periosteum, and the flap was gently turned over. The calvaria bone was exposed by flapping the periosteum and a standardized trans-osseous defect with an outer diameter of 5 mm was created in the exposed bone using a 5.0 mm trephine bar (Meisinger, Neuss, Germany) operating at 1500 rpm/min or less under continuous saline irrigation in each rat. Extreme care was exercised to avoid injury to the superior sagittal sinus and dura mater (Fig. 3A). Subsequently, the defects were sufficiently filled with following: (1) group 1: 3 mg of mRCP (n = 5) as the mRCP graft (Fig. 3B); (2) group 2: 200 mg of tibia bone (n = 5) as the bone graft in one defect each; (3) group 3: no RCP were grafted in the defect as the control group. The ablated periosteum was then repositioned and the wounds were sutured using Vicryl 4–0 (Ethicon Inc., GA, USA) (Fig. 3C).

2.5. Micro computed tomography (micro-CT) imaging and analysis

The two groups were evaluated for the total volume of newly formed bone and the bone mineral density (BMD) of newly formed bone by micro-CT analysis. Initially, *in vivo* x-ray micro-CT (Cosmo Scan GX; Rigaku Corporation, Tokyo, Japan) was used for imaging as

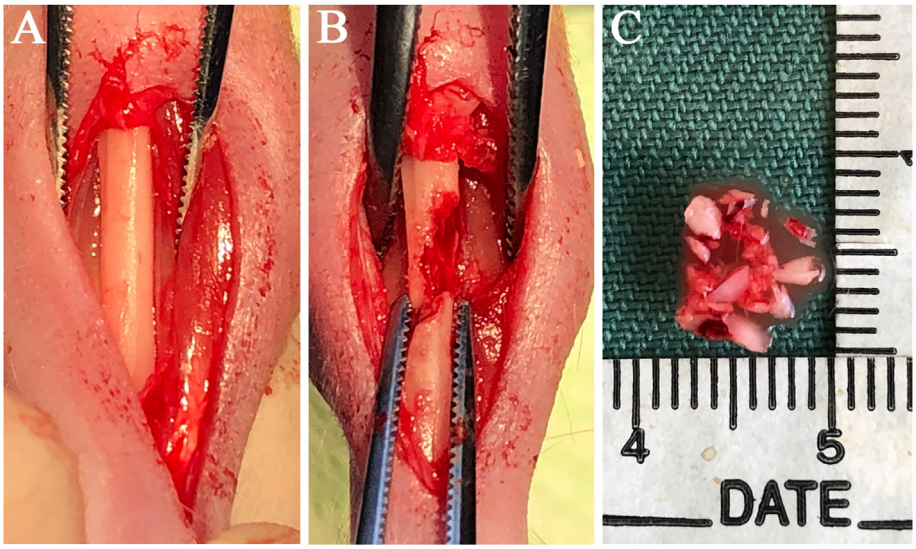

Fig. 2. (A) Gross appearance of the tibia in a T cell-deficient rat (B) Both cortical and cancellous bone were collected from the tibia for the autologous bone graft (C) The mixed bone chips were cut into small pieces (0.5–1 mm) using an osteotome.

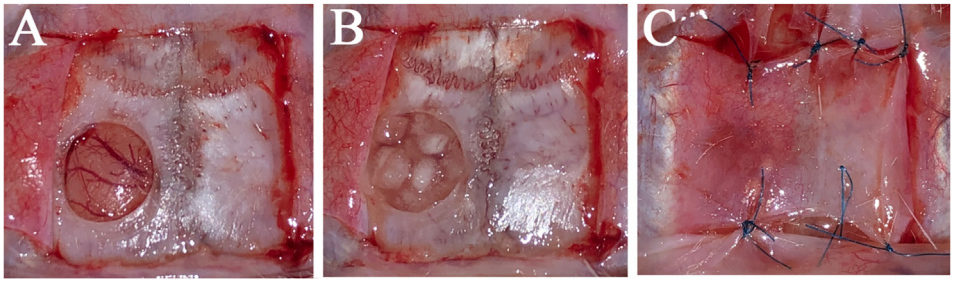

Fig. 3. (A) A 5-mm diameter bone defect made with a trephine bar in the left calvaria bone of a T cell-deficient rat (B) Three-milligram of mRCP were placed in the bone defect (C) The elevated periosteum was sutured to cover the defect with mRCP.

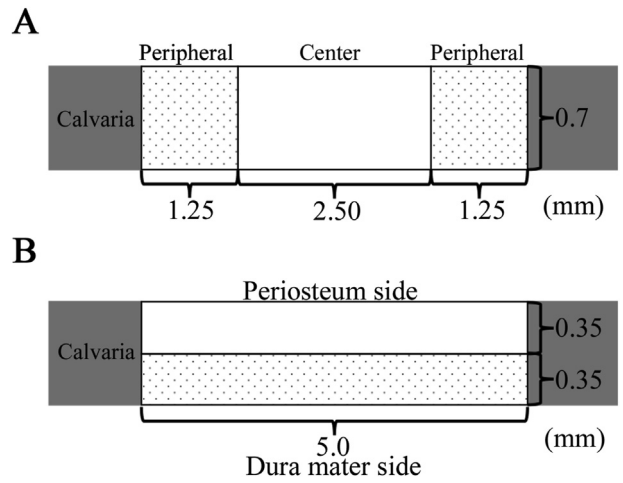

Fig. 4. (A) The level of new bone formation was calculated based on the defect width and the bone fill measurements in the central area and peripheral area of both sides (B) The level of newly formed bone was calculated based on the defect width and the bone fill measurements in the bottom side (dura matter side) and the top side (periosteal side).

described previously [44,51–54]. The exposure parameters were 18 s, 90 kV, and 100 μA. The isotropic voxel size was 45 μm. Micro-CT images were obtained from each rat before the surgery and at 1, 2, 3, and 4 weeks after surgery.

The bone volume was measured in the regions of interest (ROIs) from voxel images using the bone volume-measuring software, 3 by 4 viewer 2011 (Kitasenjyu Radist Dental Clinic i-View Image Center, Tokyo, Japan). The ROI size was 2.5 mm (radius) × 2.5 mm (radius) × 3.14 × 0.7 mm (depth) which covered the entire defect area created with the trephine bar. The increased bone volume in individual rats was calculated by subtracting the value of bone volume in the ROI measured before surgery from the subsequent values measured at 1, 2, 3, and 4 weeks after surgery.

The BMD of newly formed bone was measured at 4 weeks after surgery in two groups and was compared with the neighboring native calvaria bone. BMD values were measured to plot the calibration curve of the bone mineral content obtained by scanning a hydroxyapatite phantom (No.0802–08, RATOC, Tokyo, Japan) using the software, 3 by 4 viewer 2011 (Kitasenjyu Radist Dental Clinic i-View Image Center).

2.6. Tissue preparation

The animals were sacrificed in a carbon dioxide bath at 1, 2, 3, and 4 weeks after surgery. Histologic samples were harvested including implanted sites. The samples were fixed in 4% paraformaldehyde in phosphate buffered saline for 24 h, decalcified in 10% ethylenediaminetetraacetic acid disodium salt (Muto Pure Chemicals, Tokyo, Japan) for 8 weeks, dehydrated through a graded series of ethanol solutions, and then embedded in paraffin. The specimens were prepared as horizontal-plane sections (5 μm thick) using a microtome (Leica RM2165, Nussloch, Germany), and the paraffin sections were stained with hematoxylin and eosin (H&E) for optical microscopy. Using an optical microscope, the sections were evaluated for bone formation and integration of the reconstructed areas into the neighboring native calvaria bone.

Osteoblasts and osteoclasts within the implanted area were further visualized by histological sections independently stained with alkaline phosphatase (ALP) and tartrate-resistant acid phosphatase (TRAP) (Septsapie, Tokyo, Japan). In addition, the total number of TRAP positive cells was counted at 1, 2, 3, and 4 weeks after surgery (n = 3). However, the cells existing on the surface of newly formed bone continuously with neighboring native calvaria bone were not counted when counting the TRAP positive cells in the implanted area.

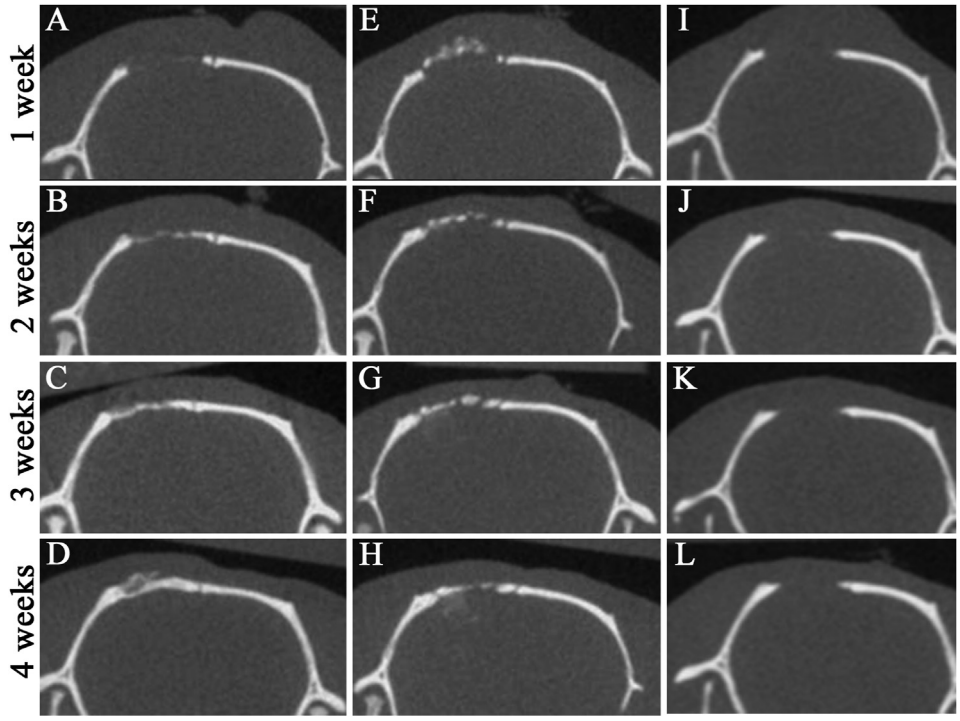

Fig. 5. Micro-CT images of the calvarial bone in the coronal plane at 1, 2, 3, and 4 weeks after implantation (A–D) mRCP grafts (E–H) Autologous bone grafts (I ~ J) No graft.

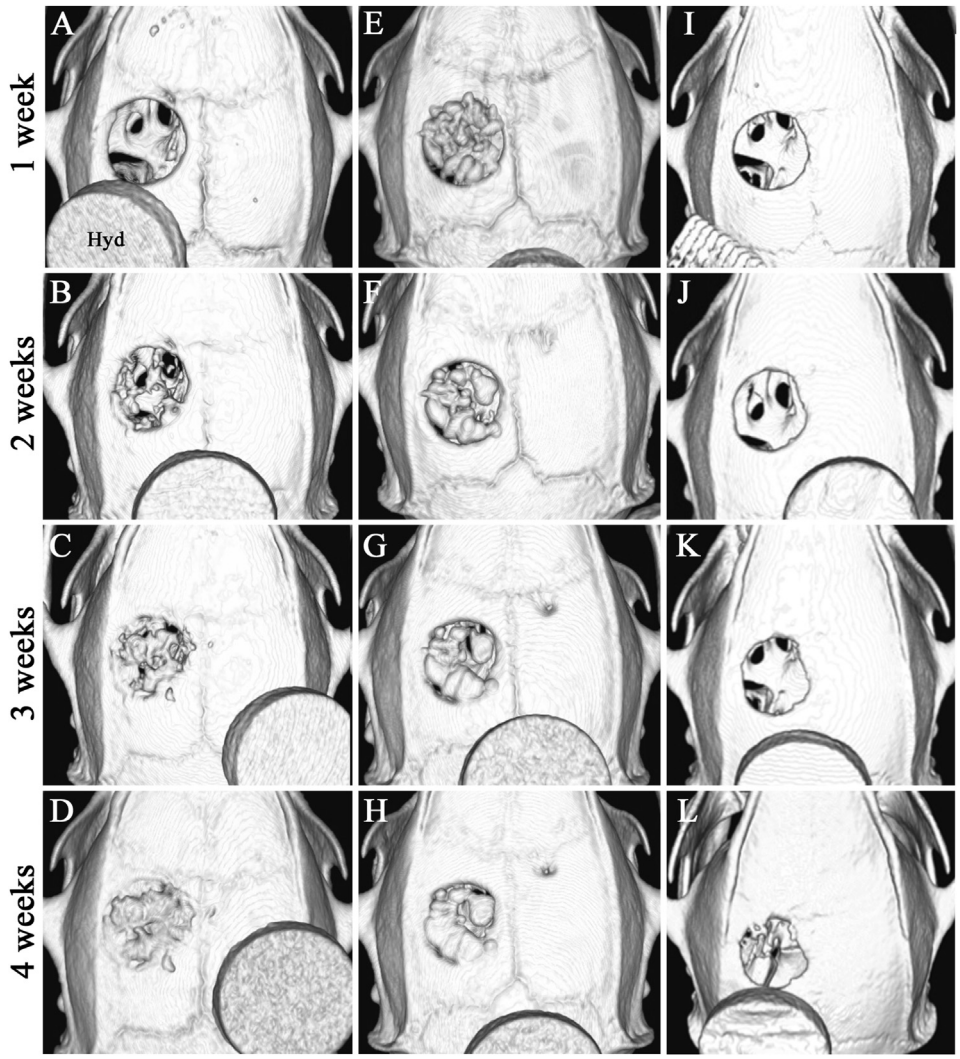

Fig. 6. Axial volume-rendered images of the calvaria bone were obtained from 3D reconstructed micro-CT images at 1, 2, 3, and 4 weeks after implantation (A–D) mRCP grafts (E–H) Autologous bone grafts (I ~ L) No graft. Hyd: Hydroxyapatite phantom.

2.7. Histomorphometry analysis

For histomorphometry analysis, an image analysis software (ImageJ software, National Institutes of Health, Bethesda, MD, USA) were used to calculate the newly formed bone area within the created bone defect area (5.0 mm × 0.7 mm) of each whole histological section, and statistical results were obtained from 3 different images at 1, 2, 3, and 4 weeks after surgery. These sections were scored via histological scoring analysis to evaluate the level of the following aspects: entire newly formed bone area, initial bone formation level, bone union level (based on new bone bridging between the newly formed bone and host bone). The level of initial bone formation was calculated based on the defect width and the bone fill measurements in the peripheral area (1.25 mm × 0.7 mm) of both the sides (1.25 mm × 0.7 mm × 2) and the central area

Table 1
Measurement of bone mineral density (BMD) by micro-CT analyses. The BMD was measured in the mRCP graft (n = 5), the autologous bone graft (n = 5) at 4 weeks after implantation, and compared with the neighboring native calvaria bone (n = 1). mRCP: medium-cross-linked recombinant peptide.

	BMD (mg/cm^3)
mRCP graft	540.1 ± 11.2
autologous bone graft	532.2 ± 14.2
native calvaria bone	544.6

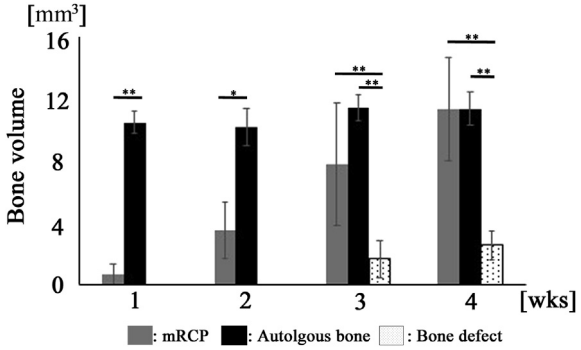

Fig. 7. Micro-CT analysis of the calvarial bone defect at 1, 2, 3, and 4 weeks after surgery. The graph shows the total bone volume of newly formed bone in the mRCP grafts, autologous bone grafts, and no graft. $^{**}P < 0.01$, $^{*}P < 0.05$. The bars and error bars in the graph represent the mean and standard deviation (SD), respectively (n = 5).

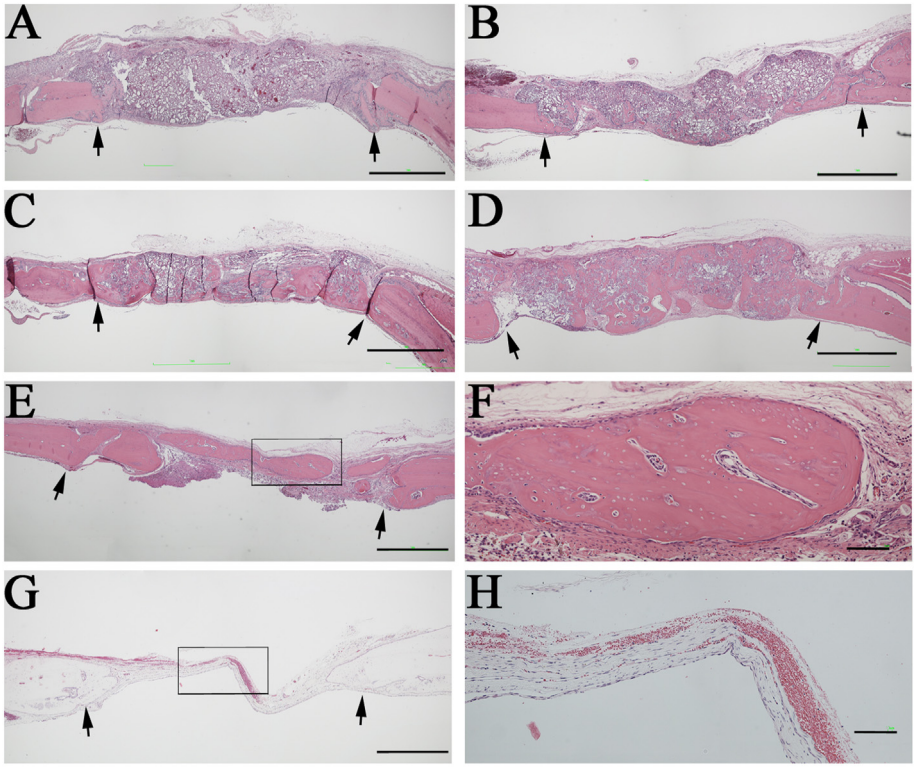

Fig. 8. Histological analysis of the rat calvaria bone. Coronal plane sections were stained with hematoxylin and eosin (H&E) at 1 (A), 2 (B), 3 (C), and 4 (D) weeks after mRCPs were grafted into the calvarial bone defect (E) Staining of autologous bone grafted into the calvarial bone defect, sectioned in the coronal plane at 4 weeks after implantation (F) Higher magnification of the framed area in E (G) Staining of no graft group into the calvarial bone defect, sectioned in the coronal plane at 4 weeks after surgery (H) High magnification of the framed are in G. Scale bars represent 1 mm (A–E) or 100 μm (F). The arrows indicate the boundary between the implanted site and the native calvarial bone.

(2.5 mm × 0.7 mm) (Fig. 4A). The level of bone union was calculated based on the defect width and the bone fill measurements in the bottom side (dura matter side, 5.0 mm × 0.35 mm) and the top side (periosteal side, 5.0 mm × 0.35 mm) (Fig. 4B).

2.8. Statistical analysis

Data are expressed as the mean and standard deviation (SD) for each group. Statistical analysis was performed using Excel Statistical File software (ystat2008. xls; Igakutosyosyuppan, Tokyo, Japan). One-way analysis of variance with a Tukey–Kramer *post-hoc* test was used for intergroup comparisons. $P < 0.05$ was considered statistically significant.

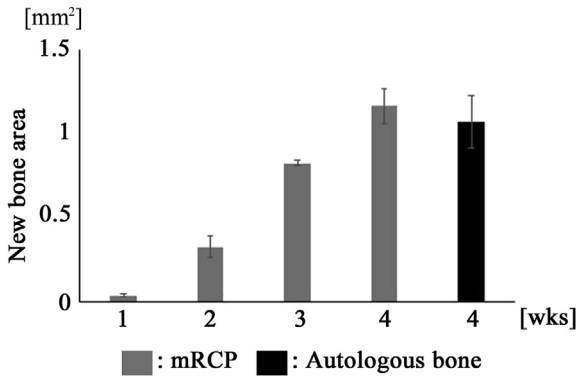

Fig. 9. Newly formed bone areas in bone defects (5.0 mm × 0.7 mm) are measured using ImageJ software at 1, 2, 3, and 4weeks after implantation in the mRCP grafts and at 4weeks after implantation in the autologous bone grafts. $^{**}P < 0.01$, $^{*}P < 0.05$. The graphs show the mean with SD (n = 3).

3. Results

3.1. Clinical results

The operative procedures were well-tolerated by all rats. No visible complications such as wound dehiscence, severe inflammation, or swelling were observed in any of the rats; the animals showed no weight reduction throughout the experimental period.

Macroscopic observation of the implanted area at 4 weeks showed hard tissue covering the bone defect and no differences in the appearance of hard tissue between both groups. Furthermore, there was no adhesion formed between the newly formed bone and the cerebral dura mater of the brain surface up to 4 weeks and the RCP fragments were smoothly detachable from the dura mater at 1 and 2 weeks after implantation.

3.2. Micro-CT measurements

To monitor the bone formation potential of mRCP compared to that of autologous bone graft up to 4 weeks after implantation, serial micro-CT analysis was performed (Fig. 5). The images of the coronal plane showed that the implanted mRCPs were visible as a faint white structure in the bone defect at 1 week (Fig. 5A). The radio-opaque area in the bone defect was gradually increased with the repair time from 1 to 4 weeks (Fig. 5A–D). At 3 weeks, the mRCP graft revealed high density covering almost the entire area of the

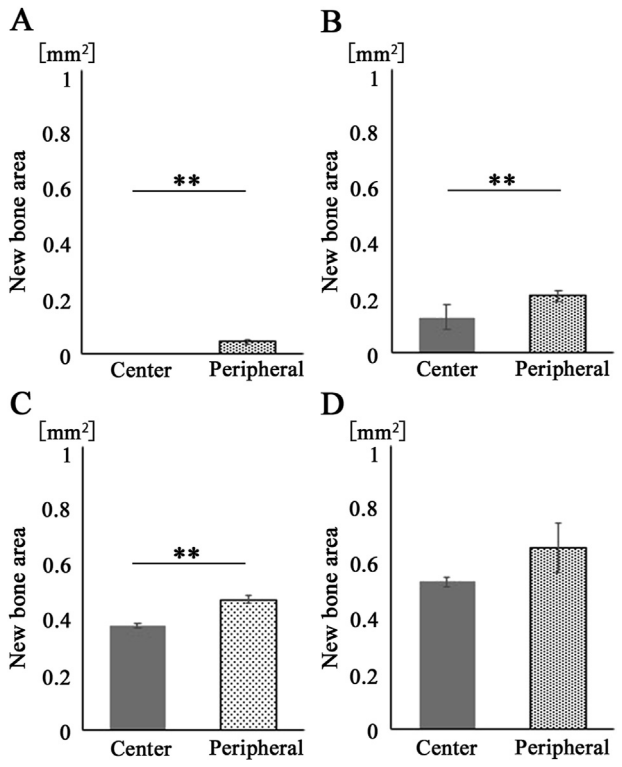

Fig. 10. Newly formed bone areas in the peripheral regions of both sides were compared with that in the central region for 4 weeks after mRCP grafting. The bone areas of the peripheral bone defect on both sides (1.25 mm × 0.7 mm × 2) and the central bone defect (2.5 mm × 0.7 mm) were measured for the entire calvarial bone defect using ImageJ software at 1 (A), 2 (B), 3 (C), and 4 (D) weeks after implantation. $^{**}P < 0.01$, $^{*}P < 0.05$. The graph shows the mean with SD (n = 3).

defect (Fig. 5C). Notably, the boundary between the regenerated area and peripheral native bone was indistinct in the mRCP graft at 4 weeks (Fig. 5D). On the contrary, the bony bridging area in the bone graft covered over half of the defect at 4 weeks (Fig. 5H). The thickness and color of the newly formed bone in the mRCP grafts was almost the same as those of the neighboring natural bone (Fig. 5D). However, no new bone formation was apparent in any samples from the negative control group at 4 weeks after surgery.

To further determine the bone formation level in the bone defect, axial volume-rendered images were obtained from 3D reconstructed micro-CT images. The images allowed visualization of considerable bony bridging at the bone defect area in the mRCP graft at 4 weeks, consistent with the images of the coronal plane (Fig. 6A–D). In the bone graft, the grafted bone chip covering the entire defect was observed at 1 week (Fig. 6E). No completed bone bridge structures had formed, and the bone structure based on several fragments was visualized in the implanted area at 4 weeks (Fig. 6H).

Since the newly formed bone was visualized in the bone defects from both groups using micro-CT, bone volume and BMD in the RCP graft were compared to those of the bone graft. There was no significant difference in the bone volume between two groups at 4 weeks, even though it was significantly less than that of the bone graft from 1 to 3 weeks after implantation (Fig. 7). BMD was measured at the point of the highest radiopacity in the newly formed bone in two groups at 4 weeks after implantation and in the neighboring native bone. No significant difference was observed in the BMD among the two groups and the native bone (Table 1).

3.3. Histological analysis of newly formed bones

Regenerated tissues within the bone defect were further visualized by histological assessment of sections stained with H&E in both groups at 1, 2, 3, and 4 weeks after implantation. The boundary between the implanted area and the neighboring native bone was easily identified in the histological images (Fig. 8A–E). The pink color of dense tissues indicated the bone that could be easily distinguished from the loose fibrous tissues and the implanted mRCP particles (Fig. 8A–F). Both groups showed bone formation indicated by the pink stained structure inside the gap, throughout the experimental period, except for the result from 1 week in the mRCP graft. The presence of a lot of mRCP particles was confirmed in the implanted area at 1 week (Fig. 8A). The newly formed bone area was measured from the histological sections using ImageJ software (NIH). There was no significant difference in the newly formed bone area within the entire implanted area between the two groups at 4 weeks (Fig. 9) in accordance with the micro-CT analysis (Fig. 7).

At 2 weeks, the newly formed bone with pink-stained structures was observed as a combination of the peripheral new bone and central new bone (Fig. 8B) in accordance with the micro-CT images in the coronal plane. The initial bone formation level was then measured in the two peripheral sides (right and left) neighboring the native bone and in the central region within the implanted area. The total bone area in the both peripheral sides was greater than that of the central region with a significant difference for up to 3 weeks, but no difference at 4 weeks (Fig. 10).

At 3 weeks the newly formed bone area with pink-stained structure in the dura matter (bottom) side was more distinguished than that on the periosteal (top) side. The bone union level

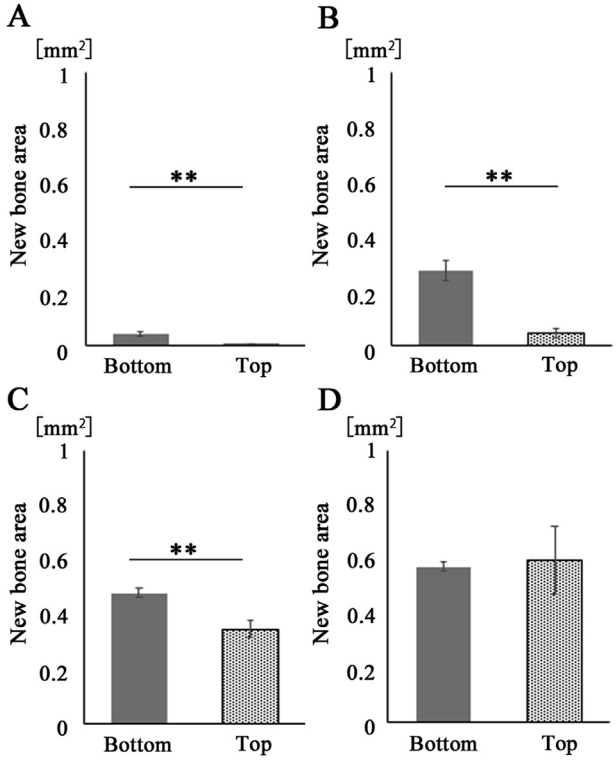

Fig. 11. Newly formed bone areas on the bottom side were compared with those on the top sides for 4 weeks after mRCP grafting. Bone areas of the bottom side and top side (5.0 mm × 0.35 mm) for the entire calvarial bone defect (5.0 mm × 0.7 mm) were measured using ImageJ software at 1 (A), 2 (B), 3 (C), and 4 (D) weeks after implantation. $^{**}P < 0.01$, $^{*}P < 0.05$. The graphs show the mean with SD (n = 3).

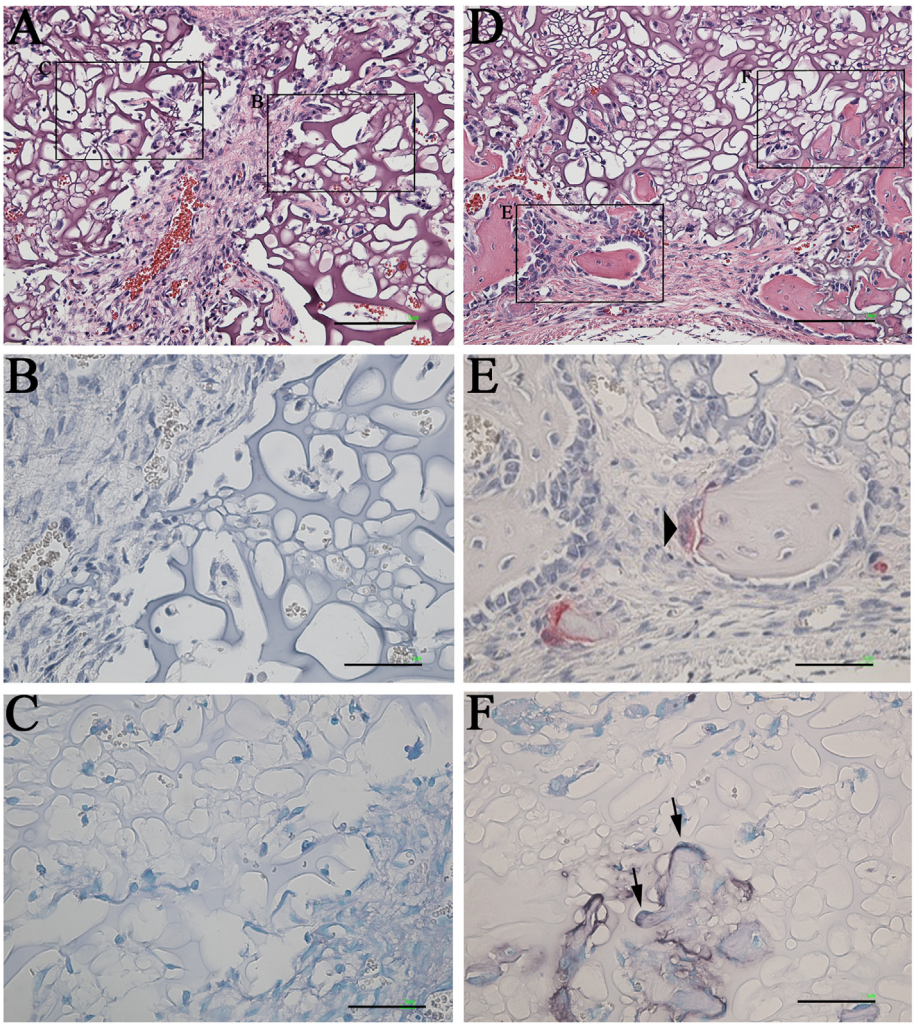

Fig. 12. Histological analysis of high-magnification images of the mRCP grafts (A) Hematoxylin and eosin (H&E) stained section of the mRCP graft at 1 week. Scale bars represent 100 μm (B) No osteoclasts were stained with tartrate-resistant acid phosphatase (TRAP) at 1 week. The image shows the boxed area on the right side in A. Scale bars represent 50 μm (C) No osteoblasts were stained with alkaline phosphatase (ALP) at 1 week after implantation. The image shows the boxed area on the left side in A. Scale bars represent 50 μm (D) H&E stained section of mRCP graft at 2 weeks. Scale bars represent 100 μm (E) Osteoclasts were stained with TRAP at 2 weeks. The image shows the boxed area on the left side in D. Scale bars represent 50 μm (F) Osteoblasts were stained with ALP at 2 weeks. The image shows the boxed area on right side in D. Scale bars represent 50 μm. Arrowhead and arrows indicate osteoclast and osteoblasts, respectively.

was the compared in both sides of the mRCP graft. The bone bridging area in the dura matter side was significantly larger than that on the periosteal side for up to 3 weeks, but was not significantly different at 4 weeks (Fig. 11).

At 4 weeks a large fraction of the implanted mRCP particles were resorbed and a large amount of the pink-stained structure was observed within the implanted area (Fig. 9D). Several bone segments were observed within the implanted area in the bone graft at 4 weeks (Fig. 8E). The segments included the cells within the bone lacunae, whereas some bone lacunae showed the ventricle in the same bone segment (Fig. 8F). No new formed bone tissue was recognized in the defect area from the negative control group (Fig. 8G and H).

TRAP/ALP staining was performed to confirm the activity of osteoblasts and osteoclasts within the implanted area in the mRCP graft (Figs. 11 and 12). At 1 week, no staining of osteoblasts and osteoclasts was observed in the mRCP graft (Fig. 12 A–C). At 2 weeks, small bone segments were observed partly, and osteoclasts and osteoblasts were recognized on the surface of the newly formed bone (Fig. 12D–F). The number of bone segments were gradually increased from 2 weeks to 3 weeks (Figs. 12C and 13A) and the size of the bone segment was increased from 3 weeks to 4 weeks (Fig. 13A and D). To determine the level of bone metabolism during the regeneration period, the number of osteoclasts was counted in the implanted area for up to 4 weeks in the mRCP graft. Although no osteoclasts were observed at 1 week, the osteoclast number gradually increased as follows; 18 cells at 2 weeks, 57 cells at 3 weeks, and 73 cells at 4 weeks in respective specimens.

4. Discussion

This study aimed to clarify whether mRCP particles have bone formation potential comparable to that of autologous bone chips under comparable healing regions in rat calvaria bone. To our knowledge, this is first report showing that mRCP particles exhibit good osteoconductive properties, with high new bone formation potential, and a high degree of direct bone apposition in the calvarial bone defect.

To date, a series of studies have been conducted on RCP materials at various facilities [27,43,55]. The mechanical properties and

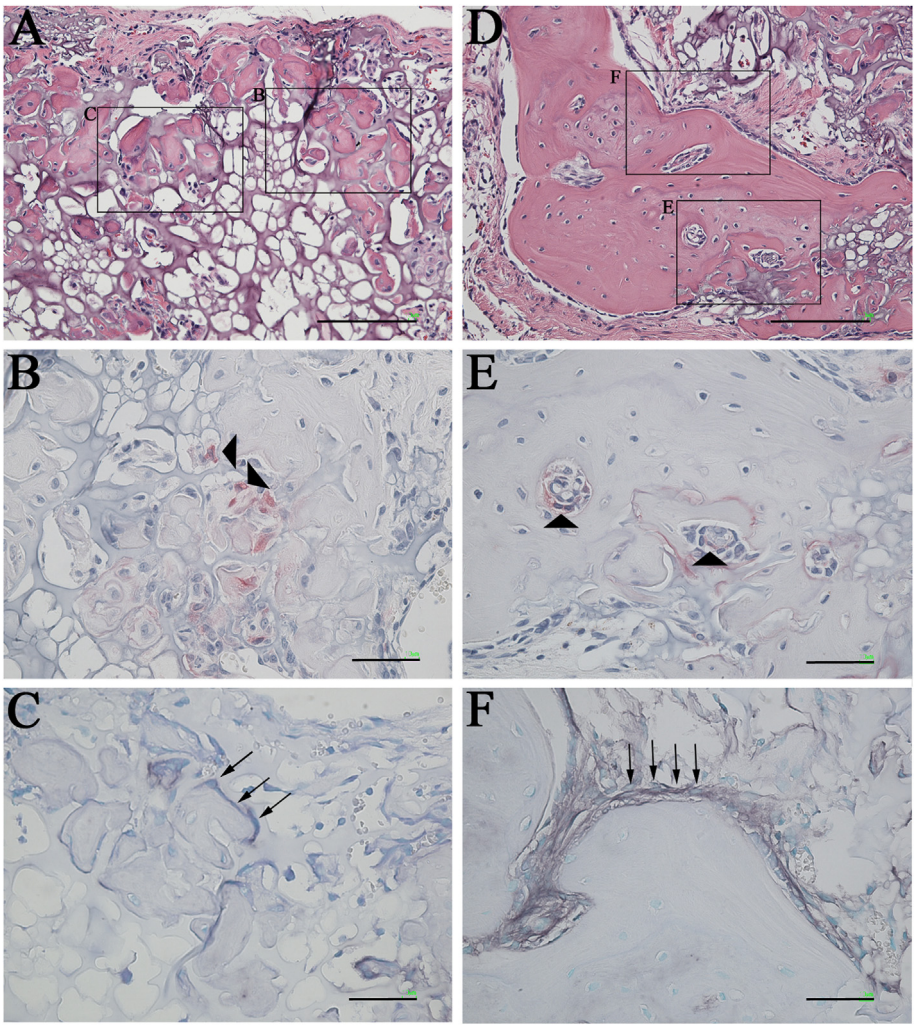

Fig. 13. Histological analysis of high-magnification images of the mRCP grafts (A) H&E stained section of mRCP graft at 3 weeks. Scale bars represent 100 μm (B) Osteoclasts were stained with TRAP at 3 weeks. The image shows the boxed area on the left side in A. Scale bars represent 50 μm (C) Osteoblasts were stained with ALP at 3 weeks. The image shows the boxed area on the right side in A. Scale bars represent 50 μm (D) H&E stained section of mRCP graft at 4 weeks. Scale bars represent 100 μm (E) Osteoclasts were stained with TRAP at 4 weeks. The image shows the boxed area at the lower side in D. Scale bars represent 50 μm (F) Osteoblasts were stained with ALP at 4 weeks. The image shows the boxed area on the upper side in D. Scale bars represent 50 μm. Arrowhead and arrows indicate osteoclasts and osteoblasts, respectively.

biodegradation rate of the bone substitutes influences the quantity and quality of newly formed bone [56]. Cross-linking of collagen-based biomaterials helps improve the mechanical properties of materials toward degradation. Cross-linking agents affect the cross-link density and stiffness of collagen-based materials, and their resistance to cell-mediated contraction has been demonstrated previously [57]. Three cross-linking methods, dehydothermal treatment (DHT), hexamethylene diiscocyanate, and genipin [29,58,59] were examined to choose the appropriate cross-linking method for producing the RCP materials used in this study. Based on the results, DHT was applied to optimize the mechanical properties of RCP materials [56,60].

The degree of DHT treatment also affects the degradation rate and is a key factor in determining the bone regeneration activity. Materials with a lower cross-link density are shown to be biodegraded rapidly whereas a higher cross-link density can resist biodegradation for a longer time. To determine the optimal cross-link density, three different densities of RCP particles with similar pore sizes and porosity were prepared in our previous study. Based on our *in vivo* results, mRCP were chosen for this study (in submission). The pore size of mRCP particles was approximately 100 μm and their porosity was approximately 80%. If the pores are too small, cell migration is limited and if pores are too large, there is a decrease in the surface area limiting the cell adhesion and mechanical properties [61]. The porous bone substitutes used for long bone repair usually have a pore size of 200–350 μm; however, the scaffolds used in long bone repair are not suitable for alveolar cleft bone repair [62]. A previous study on alveolar bone defects showed that the optimal pore size is 130 μm and that resulting the regenerative performances were quite desirable according to the *in vivo* experiments [62].

Although some studies suggest that a 5-mm diameter calvarial bone defect is not a critical-size defect (CSD) in rats, several studies have reported that a full-thickness 5-mm diameter defect is a CSD in rat calvaria [63,64]. Based on the information from previous studies, a unilateral 5-mm full thickness defect was created in the non-suture associated right parietal bone in this study. The results from micro-CT were quantified and presented as the average fraction healing of the original defect size. In our study, there was no significant difference according to the two dynamic parameters of bone volume and BMD in the newly formed bone between the mRCP and autologous bone grafts at 4 weeks post-surgery. Consistent with micro-CT

analysis, histological analysis showed that mRCP-engrafted defects showed marked bone regeneration at 4 weeks post-surgery. Taken together, the qualitative and quantitative histomorphometric analysis revealed that the bone formation potential of mRCP was comparable to that of the autologous bone graft. In addition, the results suggested that mRCP particles possess a proper balance between porosity and mechanical properties. The balance between bone formation and particle degradation may also be almost matched, but further study is needed for confirmation.

Regenerated bone within the calvarial bone defects represented a combination of central and peripheral new bone tissues in the RCP graft. The peripheral new bone density was significantly greater than the central new bone density at 2 and 3 weeks. In addition, the histomorphometry results showed that the bottom side (dura matter side) scores were significantly higher than those of the top side (periosteal side) at 1, 2, and 3 weeks. Furthermore, bone bridging was observed in the bottom side over the entire defect above the dura mater at 4 weeks. These results are consistent with the previous research outcome [62]. When mRCP were grafted into the calvarial bone defect, they came into contact with three main kinds of host tissue, the diploë layer in calvaria, dura mater, and periosteum [65–67]. A previous study showed that osteogenic potential from the calvarial diploë layer was demonstrated when the defects were protected from soft-tissue prolapse at both the dural and pericranial surface [65]. Our results thus indicate that bone production in the peripheral area may be subject to the strong osteogenic influence of the calvarial diploë layer. Furthermore, the diploë layer in calvaria may have an abundant nutritional and stem cell supply. However, dura mater cells have long been recognized to play a significant role in the intramembranous ossification of the calvaria [65,68]. A previous study showed significantly decreased mineralization rates in cranial bone grafts that were not in contact with the dura mater [68]; further, if new bone formation was reduced dramatically in the absence of either the dura or the periosteum adjacent to the calvaria defect [65–67]. Taken together, our results suggest that the dura mater appears to be the primary source of central new bone and that the dura mater pathway is more influential than the periosteum pathway. However, further studies are needed to clarify these points.

5. Conclusion

In conclusion, this study demonstrates that mRCP could be useful for alveolar cleft repair in the clinical setting because mRCP has a high potential of recruiting osteogenic cells, comparable to that of autologous bone chips.

Declaration of competing interest

This work was supported by the joint research expenses with FUJIFILM Corporation (Tokyo, Japan).

Takahiro Hiratsuka, Kazuhiro Yamaguchi, Akihiko Azuma and Ken-ichiro Hata are employees of FUJIFILM Corporation. Other authors have no conflicts of interest.

Acknowledgments

We thank Sept Sapie CO., LTD (Tokyo, Japan) for the preparation of paraffin sections and ALP and TRAP staining.

References

[1] Ali SA, Mossey P, Gillgrass T. A study model based photographic method for assessment of surgical treatment outcome in unilateral cleft lip and palate patients. Eur J Orthod 2006;28:366–72.

[2] Bajaj AK, Wongworawat AA, Punjabi A. Management of alveolar clefts. J Craniofac Surg 2003;14:840–6.

[3] Raposo-Amaral CE, Denadai R, Alonso N. Three-dimensional changes of maxilla after secondary alveolar cleft repair: differences between rhBMP-2 and autologous iliac crest bone grafting. Plast Reconstr Surg Glob Open 2015;3:e451.

[4] Shirani G, Abbasi AJ, Mohebbi SZ. Need for revision surgery after alveolar cleft repair. J Craniofac Surg 2012;23:378–81.

[5] Forte AJ, da Silva Freitas R, Alonso N. Use of three-dimensional computed tomography to classify filling of alveolar bone grafting. Plast Surg Int 2012;2012:259419.

[6] Nicholas RW, Lange TA. Granular tricalcium phosphate grafting of cavitary lesions in human bone. Clin Orthop Relat Res 1994;306:197–203.

[7] Zerbo IR, Bronckers AL, de Lange GL, van Beek GJ, Burger EH. Histology of human alveolar bone regeneration with a porous tricalcium phosphate. A report of two cases. Clin Oral Implants Res 2001;12:379–84.

[8] Lu J, Descamps M, Dejou J, Koubi G, Hardouin P, Lemaitre J, et al. The biodegradation mechanism of calcium phosphate biomaterials in bone. J Biomed Mater Res 2002;63:408–12.

[9] Handschel J, Wiesmann HP, Stratmann U, Kleinheinz J, Meyer U, Joos U. TCP is hardly resorbed and not osteoconductive in a non-loading calvarial model. Biomaterials 2002;23:1689–95.

[10] Wang Y, Bian Y, Zhou L, Feng B, Weng X, Liang R. Biological evaluation of bone substitute. Clin Chim Acta 2020;510:544–55.

[11] Liang F, Leland H, Jedrzejewski B, Auslander A, Maniskas S, Swanson J, et al. Alternatives to autologous bone graft in alveolar cleft reconstruction: the state of alveolar tissue engineering. J Craniofac Surg 2018;29:584–93.

[12] Honda MJ, Shinohara Y, Hata KI, Ueda M. Subcultured odontogenic epithelial cells in combination with dental mesenchymal cells produce enamel-dentin-like complex structures. Cell Transplant 2007;16:833–47.

[13] Tsuchiya S, Ohshima S, Yamakoshi Y, Simmer JP, Honda MJ. Osteogenic differentiation capacity of porcine dental follicle progenitor cells. Connect Tissue Res 2010;51:197–207.

[14] Honda MJ, Yada T, Ueda M, Kimata K. Cartilage formation by serial passaged cultured chondrocytes in a new scaffold: hybrid 75:25 poly(L-lactide-epsilon-caprolactone) sponge. J Oral Maxillofac Surg 2004;62:1510–6.

[15] Ando Y, Honda MJ, Ohshima H, Tonomura A, Ohara T, Itaya T, et al. The induction of dentin bridge-like structures by constructs of subcultured dental pulp-derived cells and porous HA/TCP in porcine teeth. Nagoya J Med Sci 2009;71:51–62.

[16] Akita D, Morokuma M, Saito Y, Yamanaka K, Akiyama Y, Sato M, et al. Periodontal tissue regeneration by transplantation of rat adipose-derived stromal cells in combination with PLGA-based solid scaffolds. Biomed Res 2014;35:91–103.

[17] van Tienen TG, Heijkants RG, Buma P, de Groot JH, Pennings AJ, Veth RP. Tissue ingrowth and degradation of two biodegradable porous polymers with different porosities and pore sizes. Biomaterials 2002;23:1731–8.

[18] Cuervo-Lozano CE, Soto-Dominguez A, Saucedo-Cardenas O, Montes-de-Oca-Luna R, Alonso-Romero S, Del Consuelo Mancías-Guerra M, et al. Osteogenesis induced by a three-dimensional bioimplant composed of demineralised bone matrix, collagen, hydroxyapatite, and bone marrow-derived cells in massive bone defects: an experimental study. Tissue Cell 2018;50:69–78.

[19] Kuttappan S, Mathew D, Nair MB. Biomimetic composite scaffolds containing bioceramics and collagen/gelatin for bone tissue engineering - a mini review. Int J Biol Macromol 2016;93:1390–401.

[20] Murakami S, Miyaji H, Nishida E, Kawamoto K, Miyata S, Takita H, et al. Dose effects of beta-tricalcium phosphate nanoparticles on biocompatibility and bone conductive ability of three-dimensional collagen scaffolds. Dent Mater J 2017;36:573–83.

[21] Nathanael AJ, Oyane A, Nakamura M, Sakamaki I, Nishida E, Kanemoto Y, et al. In Vitro and in vivo analysis of mineralized collagen-based sponges prepared by a plasma- and precursor-assisted biomimetic process. ACS Appl Mater Interfaces 2017;9:22185–94.

[22] Kimura Y, Inamoto T, Tabata Y. Adipose tissue formation in collagen scaffolds with different biodegradabilities. J Biomater Sci Polym Ed 2010;21:463–76.

[23] Dunn RM. Cross-linking in biomaterials: a primer for clinicians. Plast Reconstr Surg 2012;130:18S–26S.

[24] Mano JF, Silva GA, Azevedo HS, Malafaya PB, Sousa RA, Silva SS, et al. Natural origin biodegradable systems in tissue engineering and regenerative medicine: present status and some moving trends. J R Soc Interface 2007;4:999–1030.

[25] Thomason LC, Sawitzke JA, Li X, Costantino N, Court DL. Recombineering: genetic engineering in bacteria using homologous recombination. Curr Protoc Mol Biol 2014;106:1. 16.1–39.

[26] Zhu Q, Lu C, Jiang X, Yao Q, Jiang X, Huang Z, et al. Using recombinant human collagen with basic fibroblast growth factor to provide a simulated extracellular matrix microenvironment for the revascularization and attachment of islets to the transplantation region. Front Pharmacol 2019;10:1536.

[27] Nakamura K, Iwazawa R, Yoshioka Y. Introduction to a new cell transplantation platform via recombinant peptide petaloid pieces and its application to islet transplantation with mesenchymal stem cells. Transpl Int 2016;29:1039–50.

[28] Nakamura K, Tabata Y. A new fluorescent imaging of renal inflammation with RCP. J Contr Release 2010;148:351–8.

[29] Pawelec KM, Confalonieri D, Ehlicke F, van Boxtel HA, Walles H, Kluijtmans S. Osteogenesis and mineralization of mesenchymal stem cells in collagen type I-based recombinant peptide scaffolds. J Biomed Mater Res 2017;105:1856–66.
[30] Ruoslahti E. RGD and other recognition sequences for integrins. Annu Rev Cell Dev Biol 1996;12:697–715.
[31] Eto K, Puzon-McLaughlin W, Sheppard D, Sehara-Fujisawa A, Zhang XP, Takada Y. RGD-independent binding of integrin alpha9beta 1 to the ADAM-12 and -15 disintegrin domains mediates cell-cell interaction. J Biol Chem 2000;275:34922–30.
[32] Ruoslahti E, Pierschbacher MD. New perspectives in cell adhesion: RGD and integrins. Science 1987;238:491–7.
[33] Shimaya M, Muneta T, Ichinose S, Tsuji K, Sekiya I. Magnesium enhances adherence and cartilage formation of synovial mesenchymal stem cells through integrins. Osteoarthritis Cartilage 2010;18:1300–9.
[34] Chastain SR, Kundu AK, Dhar S, Calvert JW, Putnam AJ. Adhesion of mesenchymal stem cells to polymer scaffolds occurs via distinct ECM ligands and controls their osteogenic differentiation. J Biomed Mater Res 2006;78:73–85.
[35] Enomoto-Iwamoto M, Iwamoto M, Nakashima K, Mukudai Y, Boettiger D, Pacifici M, et al. Involvement of alpha5beta 1 integrin in matrix interactions and proliferation of chondrocytes. J Bone Miner Res 1997;12:1124–32.
[36] Parvizi M, Plantinga JA, van Speuwel-Goossens CA, van Dongen EM, Kluijtmans SG, Harmsen MC. Development of recombinant collagen-peptide-based vehicles for delivery of adipose-derived stromal cells. J Biomed Mater Res 2016;104:503–16.
[37] Kantlehner M, Schaffner P, Finsinger D, Meyer J, Jonczyk A, Diefenbach B, et al. Surface coating with cyclic RGD peptides stimulates osteoblast adhesion and proliferation as well as bone formation. Chembiochem 2000;1:107–14.
[38] Schliephake H, Scharnweber D, Dard M, Rössler S, Sewing A, Meyer J, et al. Effect of RGD peptide coating of titanium implants on periimplant bone formation in the alveolar crest. An experimental pilot study in dogs. Clin Oral Implants Res 2002;13:312–9.
[39] Elmengaard B, Bechtold JE, Soballe K. In vivo effects of RGD-coated titanium implants inserted in two bone-gap models. J Biomed Mater Res 2005;75:249–55.
[40] Re'em T, Tsur-Gang O, Cohen S. The effect of immobilized RGD peptide in macroporous alginate scaffolds on TGFbeta1-induced chondrogenesis of human mesenchymal stem cells. Biomaterials 2010;31:6746–55.
[41] Shachar M, Tsur-Gang O, Dvir T, Leor J, Cohen S. The effect of immobilized RGD peptide in alginate scaffolds on cardiac tissue engineering. Acta Biomater 2011;7:152–62.
[42] Miyamoto M, Nakamura K, Shichinohe H, Yamauchi T, Ito M, Saito H, et al. Human recombinant peptide sponge enables novel, less invasive cell therapy for ischemic stroke. Stem Cell Int 2018;2018:4829534.
[43] Mashiko T, Takada H, Wu SH, Kanayama K, Feng J, Tashiro K, et al. Therapeutic effects of a recombinant human collagen peptide bioscaffold with human adipose-derived stem cells on impaired wound healing after radiotherapy. J Tissue Eng Regen Med 2018;12:1186–94.
[44] Tateno A, Asano M, Akita D, Toriumi T, Tsurumachi-Iwasaki N, Kazama T, et al. Transplantation of dedifferentiated fat cells combined with a biodegradable type I collagen-recombinant peptide scaffold for critical-size bone defects in rats. J Oral Sci 2019;61:534–8.
[45] Knott L, Bailey AJ. Collagen cross-links in mineralizing tissues: a review of their chemistry, function, and clinical relevance. Bone 1998;22:181–7.
[46] Ammann P, Rizzoli R. Bone strength and its determinants. Osteoporos Int 2003;14(Suppl 3). S13–8.
[47] McNerny EM, Gong B, Morris MD, Kohn DH. Bone fracture toughness and strength correlate with collagen cross-link maturity in a dose-controlled lathyrism mouse model. J Bone Miner Res 2015;30:455–64.
[48] Oxlund H, Barckman M, Ortoft G, Andreassen TT. Reduced concentrations of collagen cross-links are associated with reduced strength of bone. Bone 1995;17. 365S–71S.
[49] Yamauchi M, Katz EP, Mechanic GL. Intermolecular cross-linking and stereospecific molecular packing in type I collagen fibrils of the periodontal ligament. Biochemistry 1986;25:4907–13.
[50] Kuroshima S, Kaku M, Ishimoto T, Sasaki M, Nakano T, Sawase T. A paradigm shift for bone quality in dentistry: a literature review. J Prosthodont Res 2017;61:353–62.
[51] Akita D, Kano K, Saito-Tamura Y, Mashimo T, Sato-Shionome M, Tsurumachi N, et al. Use of rat mature adipocyte-derived dedifferentiated fat cells as a cell source for periodontal tissue regeneration. Front Physiol 2016;7:50.
[52] Ito M, Toriumi T, Imura H, Akiyama Y, Arai Y, Natsume N, et al. Rat palatine fissure: a suitable experimental model for evaluating bone regeneration. Tissue Eng C Methods 2019;25:513–22.
[53] Iguchi S, Suzuki D, Kawano E, Mashimo T, Kajiya M, Toriumi T, et al. Effect of local bone marrow stromal cell administration on ligature-induced periodontitis in mice. J Oral Sci 2017;59:629–37.
[54] Suzuki D, Akita D, Tsurumachi N, Kano K, Yamanaka K, Kaneko T, et al. Transplantation of mature adipocyte-derived dedifferentiated fat cells into three-wall defects in the rat periodontium induces tissue regeneration. J Oral Sci 2017;59:611–20.
[55] Furihata T, Miyaji H, Nishida E, Kato A, Miyata S, Shitomi K, et al. Bone forming ability of recombinant human collagen peptide granules applied with beta-tricalcium phosphate fine particles. J Biomed Mater Res B Appl Biomater 2020;108:3033–44.
[56] Geiger M, Li RH, Friess W. Collagen sponges for bone regeneration with rhBMP-2. Adv Drug Deliv Rev 2003;55:1613–29.
[57] Lee CR, Grodzinsky AJ, Spector M. The effects of cross-linking of collagen-glycosaminoglycan scaffolds on compressive stiffness, chondrocyte-mediated contraction, proliferation and biosynthesis. Biomaterials 2001;22:3145–54.
[58] Khor E. Methods for the treatment of collagenous tissues for bioprostheses. Biomaterials 1997;18:95–105.
[59] Muzzarelli RA, El Mehtedi M, Bottegoni C, Aquili A, Gigante A. Genipin-crosslinked chitosan gels and scaffolds for tissue engineering and regeneration of cartilage and bone. Mar Drugs 2015;13:7314–38.
[60] Ma L, Gao C, Mao Z, Zhou J, Shen J. Biodegradability and cell-mediated contraction of porous collagen scaffolds: the effect of lysine as a novel crosslinking bridge. J Biomed Mater Res 2004;71:334–42.
[61] Huang H, Oizumi S, Kojima N, Niino T, Sakai Y. Avidin-biotin binding-based cell seeding and perfusion culture of liver-derived cells in a porous scaffold with a three-dimensional interconnected flow-channel network. Biomaterials 2007;28:3815–23.
[62] Wang S, Yang Y, Koons GL, Mikos AG, Qiu Z, Song T, et al. Tuning pore features of mineralized collagen/PCL scaffolds for cranial bone regeneration in a rat model. Mater Sci Eng C Mater Biol Appl 2020;106:110186.
[63] Bosch C, Melsen B, Vargervik K. Importance of the critical-size bone defect in testing bone-regenerating materials. J Craniofac Surg 1998;9:310–6.
[64] Blom EJ, Klein-Nulend J, Yin L, van Waas MA, Burger EH. Transforming growth factor-beta 1 incorporated in calcium phosphate cement stimulates osteotransductivity in rat calvarial bone defects. Clin Oral Implants Res 2001;12:609–16.
[65] Gosain AK, Santoro TD, Song LS, Capel CC, Sudhakar PV, Matloub HS. Osteogenesis in calvarial defects: contribution of the dura, the pericranium, and the surrounding bone in adult versus infant animals. Plast Reconstr Surg 2003;112:515–27.
[66] Mabbutt LW, Kokich VG. Calvarial and sutural re-development following craniectomy in the neonatal rabbit. J Anat 1979;129:413–22.
[67] Reid CA, McCarthy JG, Kolber AB. A study of regeneration in parietal bone defects in rabbits. Plast Reconstr Surg 1981;67:591–6.
[68] Hobar PC, Schreiber JS, McCarthy JG, Thomas PA. The role of the dura in cranial bone regeneration in the immature animal. Plast Reconstr Surg 1993;92:405–10.